



CHORUS

This is the accepted manuscript made available via CHORUS. The article has been published as:

Conductivity Induced by High-Field Terahertz Waves in Dielectric Material

B. D. O'Shea, G. Andonian, S. K. Barber, C. I. Clarke, P. D. Hoang, M. J. Hogan, B. Naranjo, O. B. Williams, V. Yakimenko, and J. B. Rosenzweig

Phys. Rev. Lett. **123**, 134801 — Published 23 September 2019

DOI: [10.1103/PhysRevLett.123.134801](https://doi.org/10.1103/PhysRevLett.123.134801)

Conductivity Induced by High-Field Terahertz Waves in Dielectric Material

B. D. O'Shea^{1,2*}, G. Andonian¹, S. K. Barber^{1,3}, C. I. Clarke², P. D. Hoang¹, M. J. Hogan², B. Naranjo¹, O. B. Williams¹, V. Yakimenko², J. B. Rosenzweig¹

¹*UCLA Department of Physics and Astronomy, 405 Hilgard Ave., Los Angeles, California 90095, USA*

²*SLAC National Accelerator Laboratory, Menlo Park, California 94025, USA*

³*Lawrence Berkeley National Laboratory, University of California, Berkeley, California 94720, USA*

An intense, sub-picosecond, relativistic electron beam traversing a dielectric lined waveguide generates very large amplitude electric fields at terahertz (THz) frequencies through the wakefield mechanism. In recent work employing this technique to accelerate charged particles, generation of high-power, narrowband THz radiation was demonstrated [1]. The radiated waves contain fields with measured amplitude exceeding 2 GV/m, orders of magnitude greater than those available by other THz generation techniques at narrow bandwidth. For fields approaching the GV/m level, a strong damping has been observed in SiO₂. This wave attenuation with onset near 850 MV/m, is consistent with changes to the conductivity of the dielectric lining and is characterized by a distinctive latching mechanism that is reversible on longer time scales. We describe the detailed measurements that serve to clarify the underlying physical mechanisms leading to strong field-induced damping of THz radiation ($\hbar\omega=1.59$ meV, $f=0.38$ THz) in SiO₂, a bulk, wide band-gap (8.9 eV) dielectric.

High intensity, narrowband terahertz (THz) waves [2,3,4] are burgeoning tools applied to a wide range of studies, including: excitation of bound electron-hole pairs [5]; insulator-to-metal phase transitions [6]; and high-frequency resonances in matter [7]. Further, high-gradient acceleration schemes based on wakefield excitation at THz frequencies, including dielectric wakefield accelerators (DWA), may enable advanced techniques for future particle colliders and compact, high-brightness light sources such as free-electron lasers [8,9]. Viewed as a generator of THz waves, the DWA is a coherent Cerenkov radiation (CCR) based source with unique properties: near gigawatt power in nanosecond, narrow spectral bandwidth pulses. Investigations of the THz waves at high fields have shown strong damping, reducing a theoretically expected wave-train of ~ 100 periods to an observed train of less than ten periods in the experiments of Ref. [1]. The observed damping is attributable to a change in the conductivity at fields exceeding 850 MV/m. The mechanisms underlying these limitations have fundamental implications in the understanding of THz wave behavior in materials that adversely affects both dielectric-based advanced accelerators and THz sources.

Experiments are reported here that directly probe the effects of intense THz fields in bulk SiO₂, and clarify the relevant physical processes underpinning the changes in conductivity associated with the observed damping. These investigations examine two principal classes of mechanisms causing the observed wave dissipation: high field-induced damping, and the seeding of free-carriers in the bulk dielectric by direct ionization. The experimental results and analysis indicate that the induced, temporary conductivity is notably dependent only on the dielectric's interaction with high fields, with no significant dependence on ionization of free-carriers created by direct passage of

relativistic electrons or other sources of ionizing radiation through the dielectric. Details on examination and elimination of the latter effect can be found in the Supplemental Materials [10]. Changes to the conductivity, while persisting for >100 picoseconds during the passage of the strongly damped wave train, are observed to be entirely reversed on longer time scales – measurements of the emitted radiation at lower field are identical before and after material exposure to high fields. These results and their interpretation are explored in detail below.

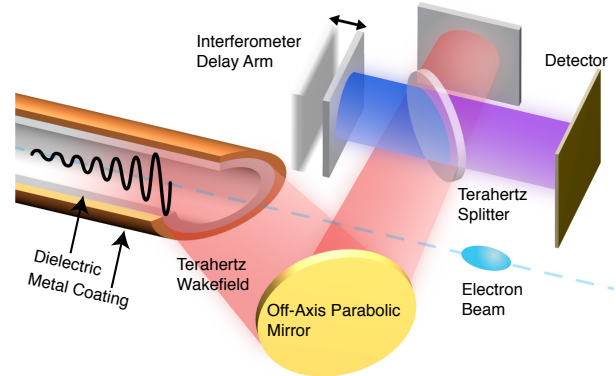


FIG. 1. An electron beam, shown in blue, traverses the dielectric-lined structure in the central vacuum region. The electron beam couples to supported modes in the structure, exciting a wakefield (shown in black). The THz wakefield is out-coupled to free space (shown in red), collimated by an off-axis parabolic mirror, and transported to a THz interferometer for spectral measurements.

Wakefields are excited through the CCR process by passing a bunched, relativistic electron beam through the on-axis vacuum channel of a dielectric-lined metallic

* boshea@slac.stanford.edu

waveguide (Figure 1) [11]. The beam couples to the longitudinal electric field E_z of the relevant eigenmodes supported by the waveguide. The amplitude of the excited wakefield is given by $|E_z| \sim \Pi_0 e N_e / \sigma_z^2$, where e is the electron charge, N_e the number of beam electrons, σ_z is the rms beam length, and Π_0 is a mode-specific field coupling parameter dependent on the dielectric permittivity, ϵ , and the structure geometry [12, 13, 14]. The wakefield group velocity, v_g , is calculated as the ratio of the power flow to the stored energy per unit length [15]. The wakefield is dominated by the fundamental mode, so the group velocity of the fundamental mode sets the expected THz wakefield length, as shown in previous work [1, 13]. In a simple cylindrical dielectric-lined waveguide, v_g is much slower than the beam velocity, v_b , ($v_g < v_\varphi = v_b \sim c$, where c the speed of light in vacuum) and the wakefield phase velocity, v_φ , matches v_b .

Intense THz waves are generated in the present experiments by electron beams provided at the Facility for Advanced Accelerator Experimental Tests (FACET) at SLAC National Accelerator Laboratory. The 20 GeV beam has a variable charge up to 3 nC, with a nominal rms bunch length of $\sigma_z = 40 \mu\text{m}$. In the measurements reported here, the beam excites wakefields in a 3 cm long, dielectric (SiO_2 , $\epsilon = 3.85$) structure having inner radius $a = 190 \mu\text{m}$ and outer radius $b = 295 \mu\text{m}$. The fundamental accelerating TM_{01} eigenmode has a resonant frequency of 384 GHz. Since the associated wavelength ($\lambda_{01} = 780 \mu\text{m}$) of this $v_\varphi < c$ mode is much longer than the bunch length, the Cerenkov wakefield is coherently excited [13]. The amplitude of the on-axis electric field, $|E_z|$, is calculated from the measured electron beam charge, a process previously experimentally benchmarked (*cf.* Ref. 1). From this on-axis field, and application of structure-specific boundary conditions, the fields in the entirety of the waveguide are determined. The magnitude of the field in the dielectric, including shielding effects at the dielectric-vacuum boundary, is $|E_d| \sim 1.1 |E_z|$. The group velocity of the fundamental mode is $v_g = 0.31c$. From these parameters, the calculated length of the THz pulse exiting the structure in the absence of damping is $L_p = L_{\text{DWA}}(c - v_g)/v_g = 6.6 \text{ cm}$ (222 picoseconds, or 85 periods).

The THz fields are experimentally characterized by measuring the autocorrelation of the emitted radiation [13] using a Michelson interferometer equipped with THz detectors (see Figure 1) [16, 17, 18, 19]. Since $v_g < v_b$, the wave train measured at the autocorrelator is proportional to the wakefield at a certain time delay behind the beam. The field at a given delay t , is $E(t) = E_0 e^{i\omega_0 t - \alpha c t (c/v_g)}$, where α is the mode loss parameter ($\alpha > 0$), and ω_0 the angular frequency. By convention, $t=0$ corresponds to the initial emission of the radiation given by the location of the drive beam centroid. This expression displays the effect of the group velocity on dissipation measurements – the time it takes for the energy to propagate is longer than indicated by

the phase information by a factor of c/v_g , and the pulse damping thus appears more accentuated in observation.

The mode loss parameter is modeled as a linear combination of three independent sources, $\alpha = \alpha_{\text{WL}} + \alpha_{\text{LF}} + \alpha_{\text{HF}}$. The first two terms are field strength-independent and arise from well-established sources of dissipation: the first, α_{WL} , from interaction of the radiation with finite-conductivity metal walls [20]; the second, α_{LF} , from the THz absorption in SiO_2 at low fields [21]. For the fundamental mode, using a model for the conductor boundary described in previous work [1], $\alpha_{\text{WL}} = 15 \text{ m}^{-1}$. The low intensity contribution to the damping from the known SiO_2 loss tangent [21] at this frequency is given by $\alpha_{\text{LF}} \sim 100 \text{ m}^{-1}$. Thus, the total expected contributions to the loss parameter are $\alpha_0 = \alpha_{\text{LF}} + \alpha_{\text{WL}} \cong 115 \text{ m}^{-1}$; there are, however, notable variations in α_{LF} that depend on specific material properties, most importantly on impurities. Figure 3 shows the measured low-field loss parameter to be $\alpha_0 = 169.8 \pm 17.1 \text{ m}^{-1}$, with the error quoted representing the 95% confidence interval here, and throughout this work. Given the expected variability of α_{LF} , this measurement is in sufficient agreement with expectations. Strikingly, however, the measured lower field conductivity is a factor of four lower than that experimentally observed in the highest field case examined here. Thus the third term, α_{HF} , is introduced to account for additional losses observed in the high field cases.

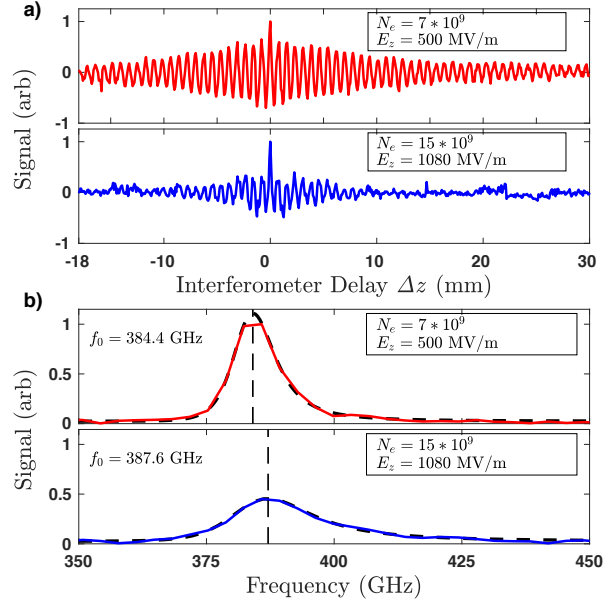


FIG 2. (a) Autocorrelation data of the CCR signal normalized to its maximum value, demonstrating loss of oscillation amplitude away from zero delay for higher charge. (b) Spectra generated via fast-Fourier transform of data from (a) shows shift in central frequency for higher field. Dashed lines correspond to Lorentzian fits.

For a wakefield that includes dissipation, the spectral line shape, $|F(\omega)|$, of the TM_{01} mode for an autocorrelation

measurement is found by taking the Fourier transform of $E(t)$. The resulting spectral line shape is approximately Lorentzian, with α and ω_0 experimentally determined by fitting to measured spectra.

The full model, including the attenuation terms, is applied to the collected data to examine the scales and sources of the observed damping in the wave train reconstruction. Figure 2(a) depicts the autocorrelation of the CCR for two data sets where the number of beam electrons is increased from 7×10^9 to 15×10^9 , corresponding to an increase in $|E_z|$ from 0.50 to 1.08 GV/m. The change in wave behavior is evident by the lack of oscillations in the autocorrelation at longer interferometer delays in higher charge cases, *e.g.* for $N_e=15 \times 10^9$ with $\Delta z = \pm 10$ mm in Figure 2(a). Figure 2(b) shows the generated radiation spectra calculated by fast Fourier transform (FFT) of the autocorrelation data given in Figure 2(a). The increase in bandwidth of the TM_{01} mode as the charge is increased reflects the growth in the loss parameter, α . Figure 3(a) shows that as the wake amplitude increases from $|E_z|=0.5$ to 1.08 GV/m the measured value of α increases from $169.8 \pm 17.1 \text{ m}^{-1}$ to $407.7 \pm 42.0 \text{ m}^{-1}$, with a high-field effect threshold observed at $|E_z| \sim 850 \text{ MV/m}$. In this range of fields, the frequency, $f_0 = \omega_0/2\pi$, changes from $384.4 \pm 3.2 \text{ GHz}$ to $387.6 \pm 7.1 \text{ GHz}$. Change in frequency, due to a decrease in the real part of the dielectric constant, is also expected from a free-carrier-derived conductivity [22]. Note that the observed frequency increase is in opposition with a frequency downshift associated with a nonlinear increase in the dielectric constant, *i.e.* due to the Kerr effect [23]. From the determination of α , this conductivity varies from $\sigma_0 = 1.69$ to $4.24 \pm 0.05 (\Omega\text{m})^{-1}$ over the range in measured field strength.

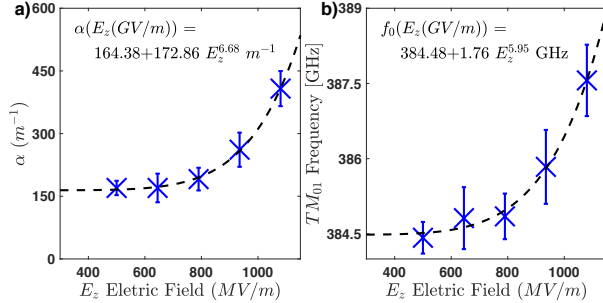


FIG. 3. (a) The loss parameter α and (b), central frequency of the excited TM_{01} mode as a function of field amplitude. Black dashed lines represent a polynomial fit to the data. Error bars represent 95% confidence interval.

The dissipative behavior found in these measurements displays two clear aspects that merit comment. The first is the presence, as noted above, of a threshold in the onset of damping near $|E_z| \sim 850 \text{ MV/m}$. The second, related, aspect is that this damping, although reversible, is latched during the wave passage; even when the amplitude of the wave decreases below threshold, the damping effect remains.

The field induced losses resulting from changes in conductivity, are directly relatable to the free-carrier density, n_0 , in the material. In dielectric materials, free-carriers can be generated through several possible mechanisms: virtual photoconductivity [24], dielectric metallization [25, 26], inter-band tunneling ionization [27] and impact ionization [28].

Virtual photoconductivity, *i.e.* polarization of a virtual electron-hole gas which results in a change in dielectric permittivity, is characterized by a very fast time scale, in the sub-picosecond (or sub-wavelength) range, due to its virtual nature [24]. However, in this experiment the conductivity clearly does not follow the instantaneous wave amplitude, but instead latches, remaining nearly constant after the wave is diminished in amplitude below threshold. This observation provides a strong counter-argument to the virtual photoconductivity hypothesis.

Dielectric metallization is a field-derived effect which has been studied for potential use in control and switching of electric currents in dielectrics. This effect has been observed at GV/m-scale fields in SiO_2 [29] using 800 nm, fs-duration laser pulses. Use of such short time-scale excitation sources permits isolation of effects occurring before collisions need to be taken into account. In contrast to the present experiments using THz waves, high-field effects arising in infrared (IR) waves possess one striking difference — the ponderomotive energy of electrons oscillating in IR fields is much smaller than the bandgap. This critically important point will be expanded upon in context of other experiments below.

The present experiments may display an adiabatic crossing of the Wannier-Stark ladder, $\hbar\omega/E_g = 1.8 \times 10^{-4} \ll 1$, provoking dielectric metallization at a relevant threshold field level $\sim 1 \text{ GV/m}$ [26]. However, the Keldysh parameter $\gamma_k = \omega_{\text{THz}} \sqrt{2m_e E_g} / eF = 2-5 \times 10^{-2}$ is sufficiently small in the present cases to suggest tunneling ionization [30,31] as a source of conduction band electrons instead of dielectric metallization. Here E_g is the bandgap energy, F the peak THz field strength, ω_{THz} the wave frequency, and m_e the electron mass. However, despite consideration of a range of material parameters, tunneling ionization calculations of conduction electrons give poor agreement with the measured results.

Finally, we discuss impact ionization, a process in which inter-band collisions excite valence band electrons to the conduction band, thus changing the bulk conductivity. In the present experiments, the excited high-field THz waves persist for time durations much longer than collisional time scales. As such, impact ionization is expected to play a significant role in the conductivity increase. This experiment's accurate measurements of field strength allow observation of instantaneous changes in electric field losses. Relevantly, the observed behavior is consistent with the known effect of suppression of impact ionization through acoustic-phonon runaway [28]. This is a material dependent effect whereby conduction band

electrons lose energy due to collisions with phonons and cannot gain sufficient energy to impact-ionize valence band electrons. Figure 3 indicates that in SiO₂, acoustic-phonon collisions prevent electrons from reaching energies sufficient to bridge the bandgap at fields below 850 MV/m. Our measurement thus shows the effect of overcoming this suppression in narrow-band THz, with a threshold field level similar to that observed using DC fields of near 700 MV/m. Additionally, it demonstrates a new effect, the latching of this damping phenomena. Here “latching” is used to describe the difference in the behavior of the material at the measured threshold when approached from above or below the threshold value. Once the threshold of 850 MV/m is exceeded, acoustic-phonon collisions do not suppress impact ionization even if the field returns below the threshold because conduction electrons with large ponderomotive energy persist while the wave field is still present, leading to impact ionization of the material. However, once the THz field is removed completely, collisional relaxation returns the material to its original behavior for excitations below 850 MV/m.

Recent work examining material photoluminescence in single-cycle THz excitations shows similar damping effects [32]. However, there are key differences in the underlying physical mechanism in the single-cycle case compared with the many-cycle wave train systems we have examined. In the single-cycle work of Ref. 35, the THz pulses are short enough to avoid phonon collisions, and they show that the intensity of electron-hole pair recombination behaves like $n_0 \propto E_{THz}^8$. Other experiments that use metamaterials on GaAs [33,34] to enhance the THz fields observe changes on short time scales in the metamaterial response attributable to increased conductivity. The results presented here extend these previous studies to examine wave train induced effects, where a major new effect, that of high-field conductivity latching, is observable.

To quantify the physical basis of the threshold and latching behavior in the experiments reported in this work, the energy of an excited carrier electron in the wake electric field, if not limited by collisions, is characterized by the cycle-averaged ponderomotive energy, $U_p = (1/4m_e)(eF/\omega)^2$ [35], which varies quadratically with the field strength, F , from 2.2 keV to 8.9 keV. These values exceed the scale of bound state energies in this system, set by the 8.9 eV band gap of SiO₂, by three orders of magnitude. We note that this is a unique feature of THz waves in the GV/m range. While GV/m fields have been employed in near-IR laser-driven dielectric-based accelerators [36], in such cases the ponderomotive energy available to a free-carrier electron is six orders of magnitude smaller, or in the meV range. Thus, narrowband THz waves enable study of collisional effects in materials in a way inaccessible in the IR.

The scale of the conductivity measured in this work, in the range of few $(\Omega m)^{-1}$, is similar to that previously measured in dielectric metallization, tunneling ionization and avalanche ionization experiments. However, the

differences with respect to the present methodology of measurement and excitation are significant. In recent metallization results [29] the conductivity is directly quantified by measuring a current across the dielectric. On the other hand, in studies of avalanche ionization [32], the population of conduction electrons is determined by measuring the number of photons produced by electron-hole recombination. In contrast, here we deduce the conductivity by measuring the change in dissipation of the radiated waves due to direct observation of wave damping in the dielectric. The method presented here allows complementary measurement of conductivity for materials that do not emit readily-measured photons at narrow bandwidth. Further, it presents a method for independent measurement of the field strengths excited in the material. Finally, the methods presented here can permit, with suitable control of experimental parameters, the measurement of both the absorption and the collision time of the material as a function of field magnitude.

In conclusion we have demonstrated key aspects of high field THz damping, observed through direct measurement of wave absorptive properties. We find that the observed changes in the conduction state of the dielectric are not a function of initial free-carriers generated via direct ionization from beam particle passage through the dielectric. We assert that the measured wave behavior, due to its latching characteristic, is not due to virtual photoconductivity. Indeed, the observed conductivity shows its onset above 850 MV/m, a level consistent with exceeding the threshold for acoustic-phonon runaway. Above threshold, the free carrier electrons can be driven to multi-keV energies, with concomitant avalanche-derived enhancement of induced conductivity.

Future investigations of these effects will center on both beam and laser-produced THz [37] excitation of dielectric structures in the GV/m regime. These studies will examine induced-conduction electron dynamics [38] through collection of recombination photons and time dependent measures of the free-carrier density. Relevant issues include electron-acoustic phonon-coupling and temperature dependence of the acoustic-phonon-scattering rate.

This work has strong implications on the envisioned use of dielectric structures for GeV/m acceleration. For instance, wakefield accelerator energy efficiency can be improved using resonant schemes of trains of bunches separated at integer multiples of the wakefield wavelength. In this way, interleaving trains of electron bunches are used for excitation of fields and for acceleration, permitting efficient energy transfer from drive to accelerating beams. Losses in the wakefields may limit the practical application of such schemes in simple DWA structures at high gradients. The analysis here shows the onset of field-based losses below a GV/m. Overcoming the difficulties presented by such losses may require use of advanced DWA structures that partly exclude the E -fields from the dielectric [39, 40]. Approaches may include use of photonic-based

accelerating structures which place the strong field regions exterior to the dielectric by judicious use of boundary conditions, such as the woodpile [40].

The authors would like to thank Prof. A. Lindenberg, Prof. D. Reis and Prof. M. Stockman for helpful discussions. The

UCLA effort on this experiment has been funded by U.S. DOE Divisions of High Energy Physics and Basic Energy Sciences under Contract Nos. DE-FG02-07ER46272, and DE-FG03-92ER40693. The SLAC effort on this experiment has been operated with funding from the United States DOE contract DE-AC02-76SF00515.

- [1] B. D. O'Shea *et al.*, *Nat. Commun.* **7**, 12763 (2016).
- [2] B. Ferguson and X.-C. Zhang, *Nature Materials* **1**, 26 - 33 (2002).
- [3] M. Tonouchi, *Nature Photonics* **1**, 97 - 105 (2007).
- [4] S. Carbajo *et al.*, *Opt. Lett.* **40**, 5762-5765 (2015).
- [5] T. Kampfrath, K. Tanaka and K. A. Nelson, *Nat. Photon.* **7**, 680-690 (2013).
- [6] M. Liu *et al.*, *Nature* **487**, 345-348 (2012).
- [7] H. Cheon, H.-j. Y. Yang, Y. A. Kim and J.-H. Son, *Scientific Reports* **6**, 37103 (2016).
- [8] B. Barish, N. Walker and Y. Yamamoto, *Sci. Am.* **298**, 54-59 (2008).
- [9] P. Emma, *et al. Nat. Photon.* **4**, 641-647 (2010).
- [10] See Supplementary Material for this publication.
- [11] K. L. F. Bane, P. B. Wilson and T. Weiland, *AIP Conference Proceedings* **127**, 875 (1985).
- [12] B. M. Bolotovskiy, *Usp. Fiz. Nauk.* **75**, 295 (1961).
- [13] A. M. Cook *et al.*, *Phys. Rev. Lett.* **103**, 095003 (2009).
- [14] J. D. Jackson, *Classical Electrodynamics 3rd Edition*, p. 310 (John Wiley & Sons, 1999).
- [15] S. Y. Park and J. L. Hirshfield, *Physical Review E* **62**.1 (2000): 1266.
- [16] See Supplementary Material for a description of how the radiation is collected and measured, which includes Refs. [17-19].
- [17] S. A. Antipov *et al.*, *Appl. Phys. Lett.* **109**, 142901 (2016).
- [18] S. N. Vlasov and I. M. Orlova, *Radiophys. Quantum Electron.* **17**, 115-119 (1974).
- [19] A. L. Stancik, *Vibrational Spectroscopy* **47**, 66-69 (2008).
- [20] D. M. Pozar, *Microwave Engineering* (Wiley, New York, 2005).
- [21] D. Grischkowsky, S. Keiding, M. Van Exter, and C. Fattinger, *J. Opt. Soc. Am. B.* **7**, (1990).
- [22] R. A. Kaindl, D. Hägele, M. A. Carnahan, and D. S. Chemla, *Phys. Rev. B.* **79**, 045320 (2009).
- [23] K. Dolgaleva, D. V. Materikina, R. W. Boyd, and S. A. Kozlov, *Phys. Rev. A* **92**, 023809 (2015).
- [24] D. S. Chemla, D. A. B. Miller and S. Schmitt-Rink, *Phys. Rev. Lett.* **59**, 1018-1021 (1987).
- [25] V. Apalkov and M. I. Stockman, *Phys. Rev. B* **86**, 165118 (2012).
- [26] M. Durach, A. Rusina, M. F. Kling and M. I. Stockman. *Phys. Rev. Lett.* **107**, 806602 (2011).
- [27] L. V. Keldysh, *Sov. Phys. JETP* **6**, 763 (1958).
- [28] D. Arnold, E. Cartier and D. J. DiMaria, *Phys. Rev. B* **49**, 10278 (1994).
- [29] A. Schiffrin *et al.*, *Nature* **493**, 70-73 (2013).
- [30] C. Zener, *Proc. Roy. Soc. London*, **145**, 523-529 (1934).
- [31] L. V. Keldysh, *Sov. Phys. JETP* **6**, 763 (1958).
- [32] H. Hirori, K. Shinokita, M. Shirai, S. Tani, Y. Kadoya and K. Tanaka, *Nat. Commun.* **2**, 594 (2011).
- [33] K. Fan *et al.*, *Phys. Rev. Lett.* **110**, 217404 (2013).
- [34] C. Lange, *et al.*, *Phys. Rev. Lett.* **113**, 227401 (2014).
- [35] H. Hirori, K. Tanaka, *J. Phys. Soc. Jpn.* **85**, 082001 (2016).
- [36] E. A. Peralta *et al.*, *Nature* **503**, 91-94 (2013).
- [37] U. Dorda *et al.*, *Nucl. Instr. Meth. Phys. Res. A* **829**, 233-236 (2016).
- [38] H. J. Queisser and E. E. Haller, *Science* **281**, 945-950 (1998).
- [39] G. Andonian *et al.*, *Phys. Rev. Lett.* **113**, 264801 (2014).
- [40] P. D. Hoang *et al.*, *Phys. Rev. Lett.* **120**, 164801 (2018).